An investigation of thin feature generation in direct metal laser sintering systems

Li Yang, Haijun Gong, Samuel Dilip, Brent Stucker

J.B. Speed School of Engineering, University of Louisville, Louisville, KY 40292

Abstract

The fabrication of metal structures with thin features (<1mm) with additive manufacturing processes is of interest for various lightweight applications. This paper investigates the geometrical and microstructural characteristics of thin features fabricated using an EOS direct metal laser sintering (DMLS) system. Both 1D and 2D thin features were fabricated using various process themes, and subsequently analyzed for microstructure geometrical characteristics. It was found that the selection of process parameters has significant influence on both the geometrical accuracy and the microstructure of the thin features. The results can be used for the further development of process guidelines for lightweight structures such as cellular structures and support structures.

Introduction

One of the most promising applications of additive manufacturing is the realization of freeform lightweight structures, which are extremely difficult with conventional manufacturing. Structures such as organic structures (e.g. bicycle frame shown in Fig.1a), periodic cellular structures (e.g. 3D re-entrant auxetic honeycomb sandwich shown in Fig.1b) and biomedical implants (e.g. hip stem insertion with porous surface as shown in Fig.1c) offer potentials for more efficient designs of lightweight structures that could achieve high performance-to-weight ratios and are thus both more cost efficient and environmentally conscious. These lightweight structures often contain features with dimensions of 1mm or smaller, which are often near the limit of the processes, especially for metal powder bed fusion based systems. It has been shown that for powder bed fusion processes, the thin feature structures often exhibit different characteristics due to the significantly altered thermal history [4, 5]. With the melting processes, depending on the energy beam scanning strategy, the size of the feature largely determines the size of the melting pool, which in turn affects the geometrical and mechanical characteristics of the structures. This becomes more significant when other process instabilities are taken into account, such as energy fluctuations, powder size and morphology, and the kinematic stalling effect at turning points for some laser based systems. In addition, due to the small feature dimensions, the thin wall or beam structures are subject to more significant thermal dissipation from the surrounding powder beds. As a result, thin features generated by powder bed fusion AM processes often include considerable amount of defects such as un-melted powder inclusions, internal voids, cracks and shape irregularities [6-9], and

their microstructure often exhibits finer grain size and metastable martensite phases, which is also different from the microstructure of bulky features [4, 5]. Furthermore, due to the small feature size, surface defects such as excessive powder sintering and surface cracks also have more pronounced effects on the mechanical properties of thin feature structures, making accurate design more difficult [6-12]. Another issue commonly encountered for such structures is the resolution limit. As the design size of the features becomes smaller, the dimensional errors become larger, and there exist a minimum feature dimension below which the process would not produce structures with practical values. Currently, there exist few papers in the literatures that investigate further into these issues. Many of the research studies on the characterization of cellular structure focused on the evaluation of topological designs [8, 13, 14] or the demonstration of design flexibility [15-17], while the relationship between the process selection and the characteristics of the limit features were largely overlooked. In some studies, cellular structures were even designed with dimensions considerably larger than the process limit in order to avoid the potential complication of analysis and focused on only the topological effects [9]. Several studies investigated the geometrical accuracy issue of pores generated by the cross-hatching pattern of thin tracks using selective laser melting processes, and demonstrated the control of pore size by varying the track patterns [18, 19]. While these works are closely related to small scale feature characterization, they were not focused on the geometry of the "solid" portion of the structure, which in fact determines its mechanical performance. Recently, Tsopanos et al. performed mechanical property evaluation for thin strut features generated under changing process parameters [20]. A range of parameters were investigated, and it was found that the dimensions of the struts varied between 180-250μm with a range of mechanical properties. In another study by Yadroitsev et al., the relationship between process parameters (laser power and scanning speed) and the thickness of the thin wall feature was investigated with a Phenix laser system, and it was found that 140μm was the smallest stable size achievable [21]. Overall, considerable studies are still needed to understand the design and fabrication limit of AM processes with the thin feature structures.

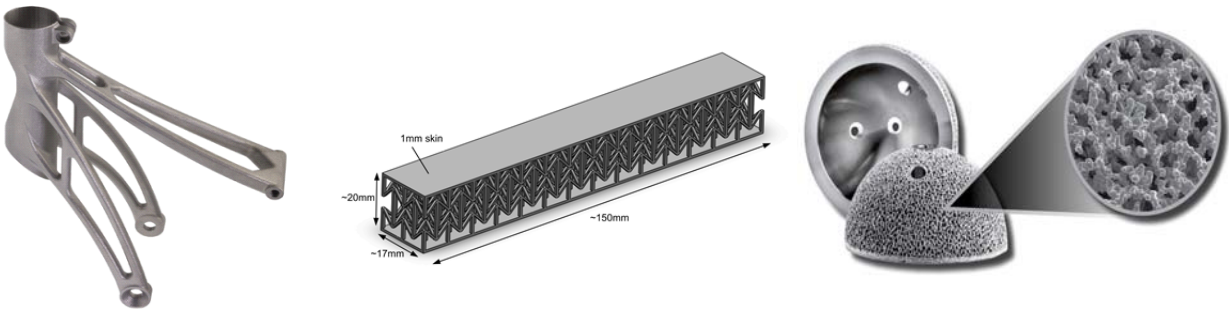

(a) Organic bicycle frame [1] (b) Re-entrant auxetic sandwich [2] (c) Hip stem insertion [3]

Fig.1 Examples of lightweight structures by AM

In this study, effort was focused on the investigation of relationships between the process parameters and the microstructure and geometry of 1D and 2D thin features with the direct metal laser sintering (DMLS) process. While EBM was considered to possess some advantages over the laser based processes for 1D thin features (e.g. cellular structures), the higher geometrical accuracy and finer resolution of the current laser based systems make it reasonable to adopt processes such as DMLS for more flexible and

accurate lightweight structure designs. On the other hand, while orientation is also another important factor that affects geometrical accuracy and mechanical strength of thin features [20, 22], it was not investigated in this study.

Process planning with DMLS

The process control of the DMLS system involves a variety of parameters and scanning strategies. For each layer, the process performs three basic scanning operations including hatch, contour and edge. As shown in Fig.2, hatch operation fills the interior region of the scanned area with a series of parallel tracks, contour operation scans along the outer contour of the scanned area, and edge operation performs a single track scanning at regions with small dimensions, such as the sharp tip of the triangular area shown in Fig.1(c). While contour and edge operations usually have fixed scanning directions, more filling strategies are available for the hatch operation, which will be illustrated in details later in this paper. These scanning operations could be used alone or in combination, which enables a variety of potential scanning strategies for different purposes, such as the density, surface quality and residual thermal stress. For regular structures with bulky geometries, a hatch operation is usually employed to create the volume of the structure, while a contour operation is employed to better define the part boundaries and improve the surface finish of the final structures. For each scanning method, there also exist multiple parameters, such as power level, scanning speed, beam offset, overhanging parameter adjustment, top/bottom skin parameter adjustment and hatch pattern adjustment. Among these parameters, power level and scanning speed directly controls the input energy density and thus the amount of material melted, beam offset compensates for the potential geometrical error caused by the characteristic energy beam size, while the other parameters are more material and geometry specific and are mostly trigger logics for the in-process adjustment of energy density.

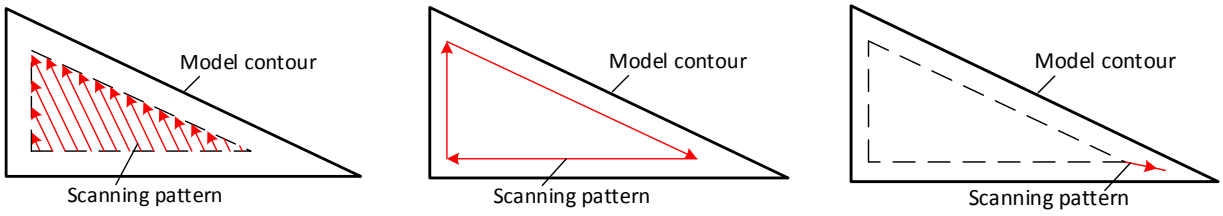

(a) Hatch (b) Contour (c) Edge

Fig.2 Basic scanning methods in DMLS

In order to investigate the scanning strategies for thin features, beam energy, scanning speed and beam offset need to be investigated systematically. Due to the small feature dimensions, parameter adjustment at different regions of scanning area is not needed, therefore the overhanging parameter adjustment and top/bottom skin parameters were not pursued in this study. While beam energy and scanning speed are common concepts for powder bed fusion processes, the definition of beam offset in the DMLS process needs further clarification. For the EOS DMLS systems, there exist two beam offset compensation parameters, which are the laser beam size offset (O_1) and the user defined in-process beam offset (O_2). The first offset is largely determined by the laser optics and material powder characterization, and is analogue to the tool diameter offset in the CNC machining process. This offset

value is usually pre-determined and fixed once a system is calibrated. The second offset is associated with the custom adjustment necessary for different geometries and energy requirements, and therefore could vary with each design. As shown in Fig.2(a), in the hatch operation, the total offset determines the distance between the outer boundary of the scan pattern and the contour of the CAD model, and the value of the total offset is determined by the sum of the two offset values. For example, for GP1 stainless steel, the standard laser beam size offset O_1 is 0.06mm, and the standard in-process beam offset O_2 varies between 0.015mm-0.04mm depending on the layer thickness, therefore, the total offset value for the hatch operation of this material is 0.075-0.10mm. For the contour operation, the same rule of total offset calculation also applies, as shown in Fig.3(b). For the edge operation, the determination of offset uses different rules. As shown in Fig.3(c), in the edge operation, the laser beam would perform single track scanning along the central line of the contour profile. The offset value of the edge operation is defined as the normal distance from the start/end point of the scanning path to the boundary of the minimum feature of interest. Therefore, in the case of a sharp angle feature, this offset is determined as the distance between the endpoint of the scanning line and the tip of the model angle contour. It is worth noting that for the calculation of offset values, the reference points from the model contour are always taken from the corners. For example, for a rectangular extrusion shown in Fig.3(d), the offset distance is calculated as the distance between the tip of the scanning path and the corners of the model contour.

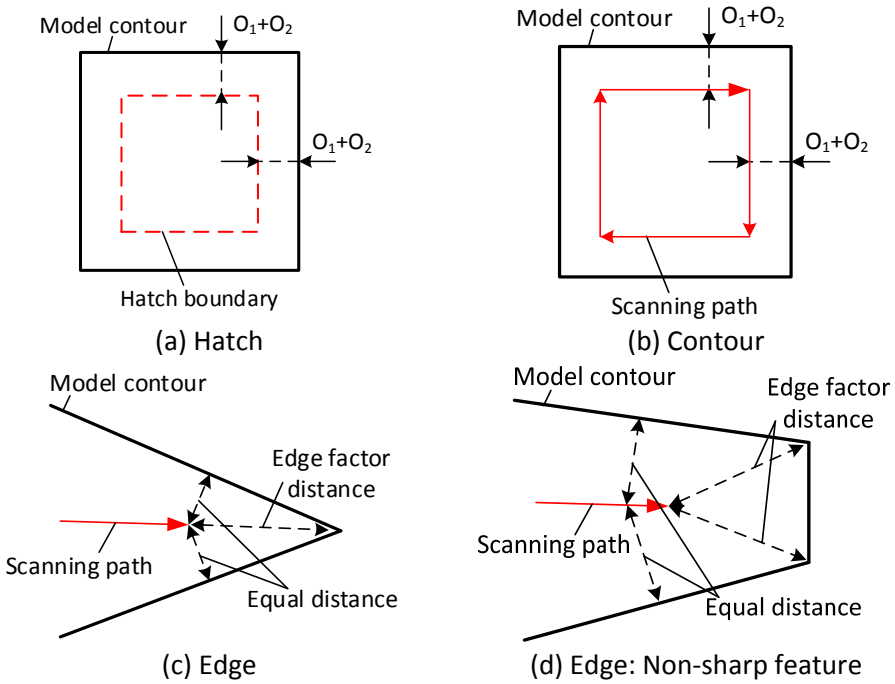

Fig.3 Offset definitions of the scanning methods

In the EOS PSW3.4 control software, the edge operation is always associated with the contour operation, and some of the parameters used to control the contour operation also affect the edge operation. There are several unique parameters for edge operation control, including edge factor (EF), threshold (TH),

radius factor (RF) and beam offset (BO), which are shown in Fig.4(a) as they appear in the control panel. The total maximum offset distance (O) from the model contour is calculated by

$O = EF \times (BO+O_1)$ (1)

Note that in the calculation, the laser beam offset O_1 is also taken into account. Eq.(1) does not include the radius factor, which could also affect the total offset distance when an angular feature is treated. Fig.4(b) shows the definition of radius factor. With radius factor = 1, the scanning path would ensure that the profile of the laser beam is completely contained within the model contour regardless of the actual edge parameter setting, while for radius factor =0, the scanning would completely ignore this factor. For simplicity, this factor was not considered in the current study, and the radius factor was set to 0 accordingly.

Another function of the offset values is to determine the maximum allowable distance from the edge scanning path to the model contour on the sides. The edge scanning path is always defined as the median line between two sides of the model contour. However, when the distance between this median line and the two sides exceeds the total offset value ($BO+O_1$), no edge scanning path will be created. Therefore, in the determination of the BO value, care must be taken to ensure that the value is at least as large as half of the width of the largest regions that requires edge operation.

The value of edge factor is determined in a less intuitive way. The PSW uses the threshold value to achieve an edge factor value selection control as:

$$\begin{cases} EF = 1.45 & when \quad TH \times (BO + O_1) < d_{contour} \\ EF = \text{set value} & when \quad TH \times (BO + O_1) \geq d_{contour} \end{cases} \quad (2)$$

where $d_{contour}$ is a distance defined by the PSW3.4 software. An attempt to identify the source of this value wasn't successful, however, Eq.(2) clearly showed that the minimum value of EF allowed in the software is 1.45, which indicates that the minimum achievable offset distance for the edge operation is always 1.45 times the total offset value. This is further illustrated in the example shown in Fig.4(c). Assume that the distance $d_{contour}$ is 0.5mm, if the TH x ($BO+O_1$) value is larger than 0.5mm, then the EF value will be automatically set as 1.45 by the process control regardless of the user setting. As a result, the offset distance of the edge scanning path will be set at 1.45 x ($BO+O_1$) following Eq.(1). On the other hand, when TH x ($BO+O_1$) value is smaller than 0.5mm, then the EF value will be taken as the actual value set by the user. Fig.4(c) showed the resulting offset distance for both cases. For the current study, it was desired to minimize the EF value for better accuracy. Therefore, the threshold value was set as TH=0 for all the experiments.

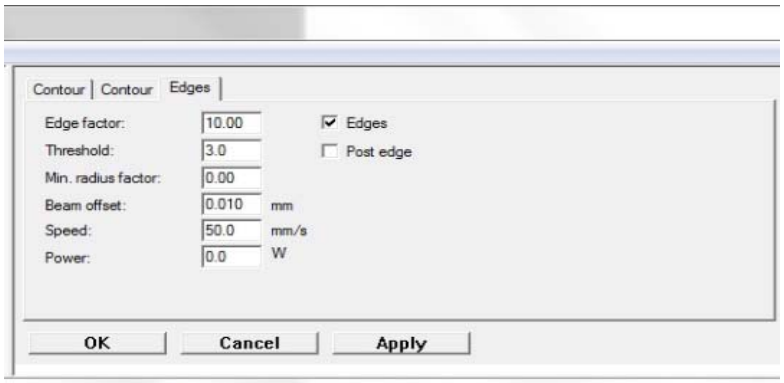

(a) PSW control parameters

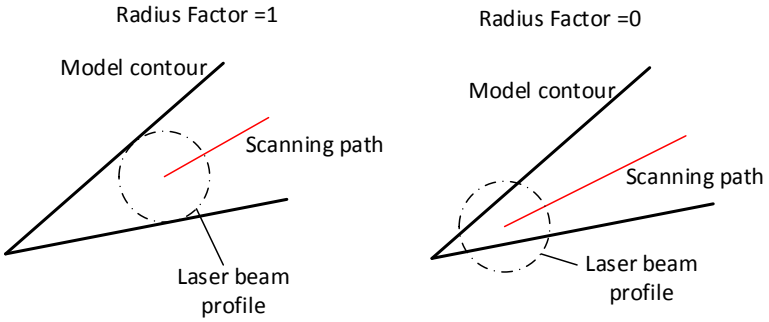

(b) Radius factor

(c) Edge offset illustration

Fig.4 Edge operation parameters

Ideally, in order to achieve smaller feature sizes, single track scanning should be adopted. With each additional scanning path, more energy input and heat dissipation is generated, therefore scanning is more likely to result in oversized feature and more significant surface sintering effect. In the generation of support wafer structures in the DMLS systems, the geometries of the support ribs are represented by vector lines in the model file, and the process performs a single track scanning operation to generate the support structure. The resulting support wafer structures are networks of thin walls perpendicular to the build direction as shown in Fig.5. The thickness of the support walls are normally between 130-200μm, and the thin wall structures also possess some mechanical strength since they serve the purpose of restricting thermal distortions of the parts. Therefore, the support structures could be used as a baseline for thin feature process development. On the other hand, the use of 2D line vectors in the representation of support structures limits the possible geometrical designs to vertical extrusions of 2D

line networks. When more complex thin feature geometries such as cellular structures are fabricated, the same process theme could not be used, and different energy densities might also be needed.

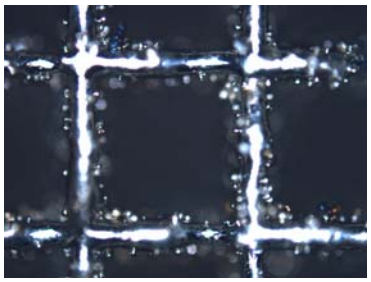

Fig.5 Support structure generated by standard DMLS process

From Fig.3 and Fig.4, it is apparent all three scanning operations could potentially be used to generate the thin features, however, each of them have their own characteristics and limitations. The contour operation will always result in a closed loop scanning path, which means that for small features the laser would scan the same area twice. Therefore, the use of contour operation should only be enabled when the feature size is above a certain threshold if single track scanning is desired, and this threshold should to be related to the effective heat affected zone of the laser beam at a certain energy density level. On the other hand, since the scanning path of the contour operation always follows the actual contour of the model, it produces more accurate shape representation. In comparison, the hatch operation could introduce considerable errors due to its controlling method. As shown in Fig.6, in the PSW3.4 control software, the positions of the hatch pattern lines are predetermined by the process envelope, which is not dependent on the locations of the fabricated models. The spacing between the hatch pattern lines is 0.1mm by default, and the angle of the pattern could be changed from layer to layer to minimize thermal distortions. The actual hatch scanning lines are generated by taking the intersections of the hatch pattern and the model areas, which in effect creates a “step effect” for the feature resolution. For features with sufficiently large dimensions, a large number of hatch lines will be generated by this algorithm, and the relative error caused by the hatch line step effect would be negligible. However, for features with dimensions comparable to the hatch pattern spacing, the actual location of the model contour could significantly affect the hatch scanning line generation, which potentially results in both dimensional and positional error for the final shape, as is illustrated in Fig.6(b). Therefore, the hatch operation should only be used for features above certain threshold dimensions, and it should be used in combination with a contour operation to better represent the shape of the processed geometries.

(a) Large features (b) Small features

Fig.6 Hatch scanning path generation in DMLS process

Based on the characteristics of each type of scanning methods, a preliminary scanning strategy could be designed that ensures full hatching of the processed area with minimum overlap scanning. The laser beam offset O_1 was used as the characteristic dimensions that would result in a fully dense structure and good cross-track bonding, since it was developed by the manufacturer. For the EOS M270 system and GP1 stainless steel (EOS GmbH) used in the current study, the default value of laser beam offset O_1 is 0.05mm. Therefore, it was assumed that the effective beam diameter is 0.1mm for this material setup. The designed scanning strategy is shown in Fig.7. For thin features with dimensions larger than 0.3mm, a combination of contour and hatch operations was used, since either the contour or the contour and edge combination could not produce a fully dense hatching pattern. For thin features with dimensions between 0.3mm and 0.2mm, a combination of contour and edge operations was used. It's worth noting that for thin features with dimensions between 0.3mm and 0.1mm, no scanning method was found to be able to achieve full hatching without creating overlapped scanning areas, as shown in Fig.7(c). On one hand, while the contour operation would cover the full area, it also results in double scanning at the center strip area. On the other hand, the edge operation would create a single track scan of the area, but would result in potentially undersized feature. Due to the limitation of the software, in the current study, the contour + edge operations were applied to features between 0.1mm and 0.3mm. Finally, for the feature size smaller than 0.1mm, only edge operations would be applied, which would result in the same effective feature size regardless of the actual dimensions. The corresponding beam offset values for this strategy are O_2=0 for hatch and contour, and BO=0.15mm for edge.

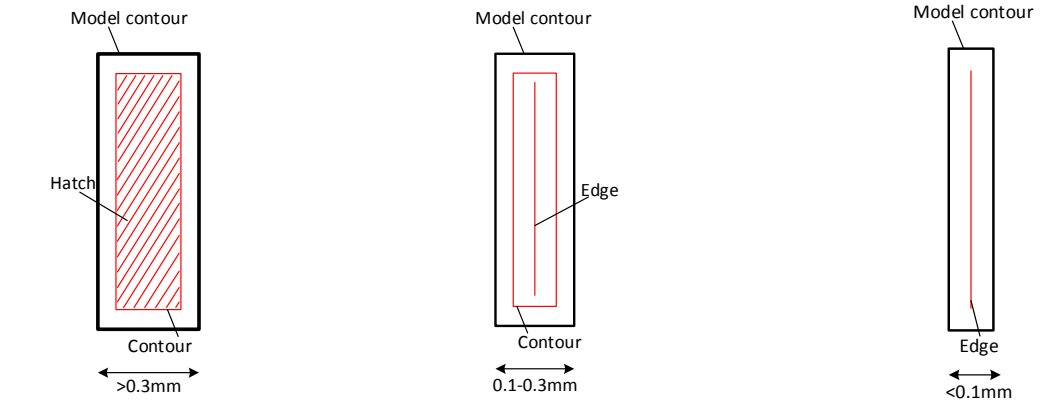

(a) Contour + hatch (b) Contour + edge (c) Edge only

Fig.7 Scanning method planning for thin feature experiment

In common practices, contour and edge operations are usually used as a secondary scanning process to achieve partial re-melting of the boundaries of the scanned areas in order to improve the geometrical accuracies. Therefore, the default contour and edge parameters were not designed intentionally to achieve direct feature generation from the powder bed. Similarly, the default hatch parameters were also optimized for full density bulky features, and might not be suitable for thin feature generation. Table 1 lists the default parameters currently recommended by EOS for GP1 stainless powder at 40µm layer thickness. There exist significant differences between different sets of parameters, and from the energy density perspective, the contour and edge parameters used for the standard practice appeared to be insufficient for direct feature fabrication. The parameters of hatch were selected as the baseline for further investigation, since it resulted in full density and good part integrity for bulky structures. In addition, the parameters of support were also used for comparison due to the fact that it generates support features with dimensions of 130-200µm as described previously (Fig.5). In fact, the energy density for support operation appears to be larger than the hatch operation, therefore the thin feature effect is likely contributed by the smaller laser power used.

Scanning method	EOS recommended		
	Laser power (W)	Scanning speed (mm/s)	Beam offset (mm)
Hatch	195	750	0.015
Contour	60	700	0.02
Edge	60	700	0
Support	70	200	-

Table 1 Default fabrication parameter setup

Experiments and results

In the first iteration, the default hatch parameter set was investigated for the direct thin feature fabrication. Power level of 195W and scanning speed of 750mm/s was used for all the scanning methods. It was expected that this parameter set would result in features with minimized interior defects. The test part for 1D and 2D thin features are shown in Fig.8. Note that in this study a 1D thin feature refers to thin wall feature, and a 2D thin feature refers to thin struts. The detailed designs for the feature size are shown in Table 2. 1D and 2D thin features with dimensions ranging from 0.01mm to 0.40mm and 0.09mm to 0.40mm were designed respectively. Each design was fabricated by three scanning methods (hatch only, contour only, and contour+edge). Note that the scanning methods used for these designs were slightly different than the optimized method.

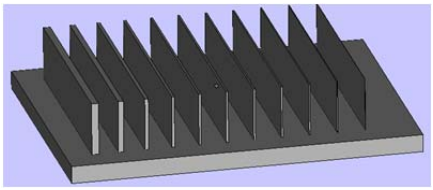

(a) 1D thin feature

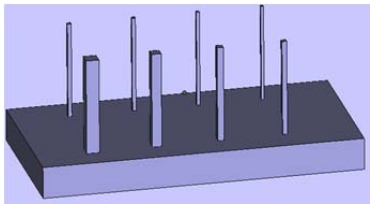

(b) 2D thin feature

Fig.8 Thin feature test sample designs

Design	Feature size (mm)
1D thin feature	0.01, 0.05, 0.07, 0.09, 0.10, 0.11, 0.12, 0.15, 0.20, 0.30, 0.40
2D thin feature	0.09, 0.10, 0.11, 0.12, 0.15, 0.20, 0.30, 0.40

Table 2 Thin feature experiment design – 1st iteration

The samples were fabricated in one batch, and were inspected under an optical microscope for dimension measurement. Due to the surface sintering effect, the dimension of the thin feature was not uniform, therefore, the maximum inclusive dimension of the feature was taken as the measurement shown in Fig.9. This treatment has been found to provide relatively accurate approximation for mechanical property evaluation [10]. Fig.10 shows the samples fabricated via different scanning methods. Some of the small size thin features were not retained in the final parts fabricated by contour and hatch scanning methods, which were primarily caused by the absence of laser scanning as analyzed previously. With the contour+edge scanning method, all the features were generated. However, it could be visually recognized that the feature dimensions were rather rough and inconsistent. Also, with the contour+edge scanning method, there was no significant dimensional difference between features with design sizes smaller than 0.12mm. The minimum 1D and 2D feature dimension obtained with the EOS default melt parameter were 100µm and 130µm respectively. It is worth noting that the minimum thin wall feature exhibited significant overall distortion, which indicated that it did not possess sufficient strength and might be deformed during the powder spreading.

Fig.9 Definition of feature dimension for thin features

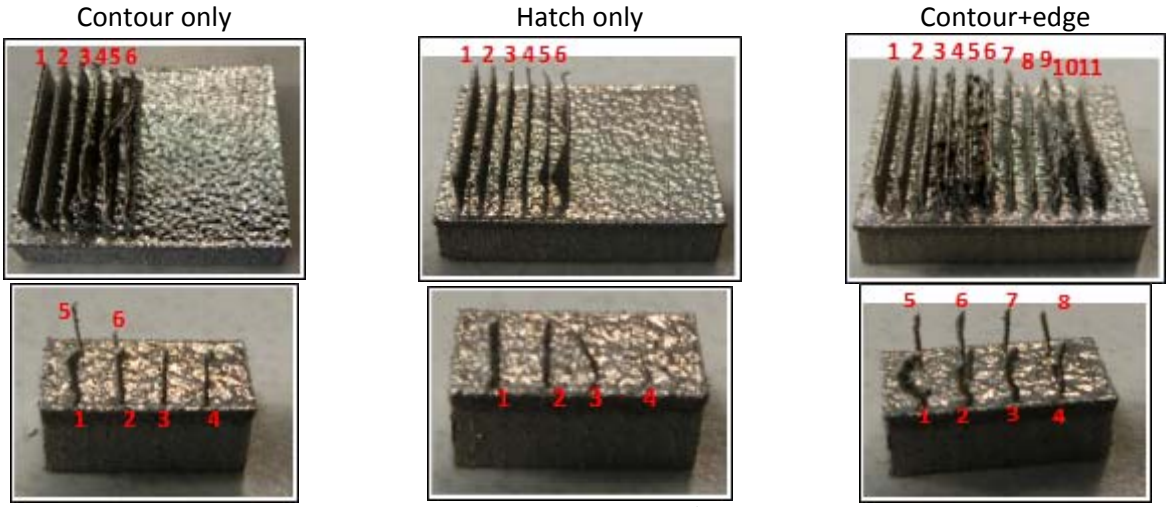

Fig.10 Fabricated samples- 1st iteration

Through this experiment, it was concluded that the default EOS parameter used for bulk geometries could not satisfy the requirement for thin feature fabrication. It was speculated that the thin feature resolution could be achieved by further reducing the energy density or the laser power. In order to verify this hypothesis, a second iteration of experiments was performed. A single track study was carried out to study the minimum feature dimension and melting pool stability for 1D thin features. Multiple energy density levels and multiple power levels were evaluated as listed in Table 3. The energy density levels corresponded to 30%, 40%, 50% and 67.5% reduction of default energy input density, and the laser power levels corresponded to 33%, 49% and 70% reduction of the default laser power. The laser was set to perform single pass scans on a 40µm layer with different parameter sets. A full factorial experiment was performed, and the fabricated tracks were inspected under an optical microscope for dimensional and stability analysis.

Parameter	Values
Energy density index (J/mm^2)	0.098, 0.13, 0.156, 0.19, 0.26
Laser power (W)	60, 100, 143

Table 3 Single track experiment design

Fig.11 shows the experimental results. Since only one layer of power was processed directly on the substrate, the heat dissipation during the process was expected to be significant due to the heat sink created by the volume of the substrate. On the other hand, if the layer was fabricated on top of a thin wall feature, then the heat dissipation would be more restricted and unidirectional. Therefore, it was also expected that the melting pool stability from single track experiments would be somewhat worse than the actual cases. However, one parameter set (60W, 230mm/s, energy density index =0.26J/mm^2) was very close to the default support parameter used by EOS, therefore it could be used as a reference for comparison, since it is known that the default EOS support parameter is quite stable for the generation of thin wall features.

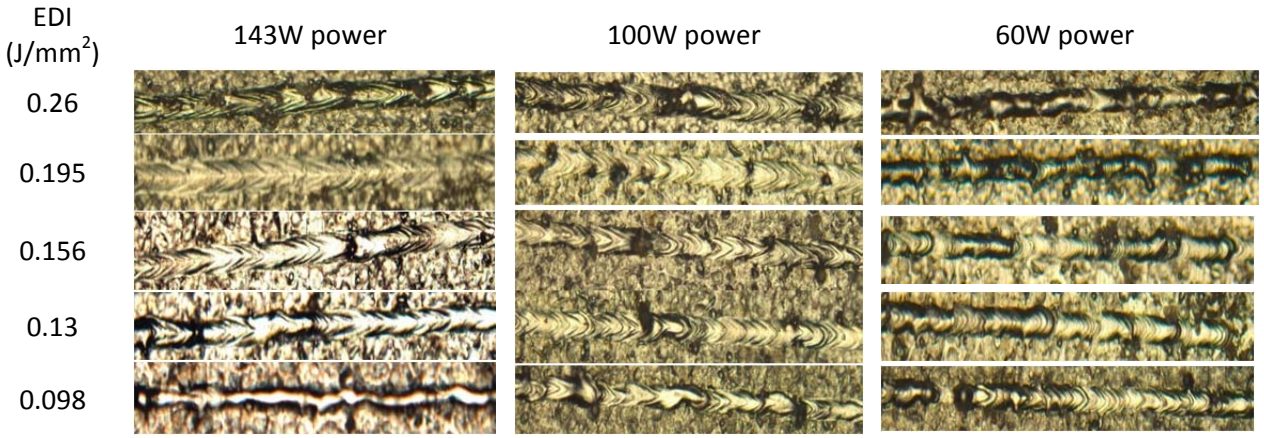

Fig.11 Single track experiment result

From Fig.11, some general trends could be clearly observed. With larger energy density, the width of the single tracks also becomes wider, which can be contributed to the large thermal affected area and therefore the larger amount of powder processed. Also, very small energy density tends to increase scanning track instability, which is likely caused by insufficient energy input and the short lifetime of the melt pool at each location. It was noticed that the default EOS parameter set did not result in satisfactory single track stability compared to the lower energy density index groups of 0.195J/mm^2 and 0.13J/mm^2. Considering both the single track stability and the observation that smaller energy density results in smaller feature size, the two groups of energy density (0.195J/mm2 and 0.13J/mm2) that exhibited best track stability were further investigated.

The experimental design of the third iteration is listed in Table 4. Samples with 1D and 2D thin features similar to the ones shown in Fig.8 were designed. The thin feature dimensions were set to be 0.1mm-0.5mm with 0.1mm increments in order to capture the trend while maintaining a relatively small sample size. Both 1D and 2D thin features were fabricated with each parameter set. According to the analysis, for 0.4mm and 0.5mm features, the contour+hatch scanning method was used. For 0.3mm features, both the contour+hatch and the contour+edge scanning method were used in order to compare them directly. For 0.1mm and 0.2mm features, the contour+edge scanning method was used.

Design	Values
Energy density index (J/mm^2)	0.13, 0.195
Laser power (J)	60, 100, 143
Feature size (mm)	0.1, 0.2, 0.3, 0.4, 0.5

Table 4 Thin feature experiment- 3rd iteration

The fabricated samples were inspected by optical microscopy for dimensional accuracies. After the inspection, the samples were also sectioned and mounted to evaluate their microstructures under an optical microscope. All the features were successfully generated, however the 0.2mm 2D thin features which were generated by the contour+edge scanning method showed consistent quality issues. As shown in Fig.12, for 0.1mm and 0.3mm thin strut features, the contour+edge scanning method generated straight strut features. However, for 0.2mm thin strut features, significant sectional

displacement occurred, and it appeared that during the process sections of the struts were displaced, which resulted in the “stacking” of short strut sections in a tilted manner. This issue was observed for all the 0.2mm 2D thin features regardless of the actual process parameters used. This issue might be caused by the unfavorable thermal history and the subsequent low strength of the struts, which was more inclined to shear displacement during the powder deployment process by the moving rake. As further illustrated in Fig.13, for an effective beam diameter of 0.1mm, the contour and edge scanning path would start to overlap when the feature size is smaller than 0.3mm. With 0.2mm feature size the overlap between the two paths achieves maximum value (0.5mm), which means potentially significant overheat in the cross section. The overheat might result in slow cooling of the scanned area and consequently lower mechanical strength which allows the strut to be plastically displaced during powder deployment.

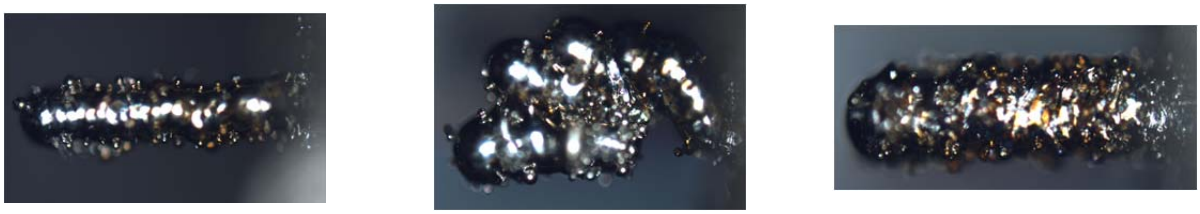

(a) 0.1mm (b) 0.2mm (c) 0.3mm

Fig.12 2D thin feature fabricated by contour+edge scanning method

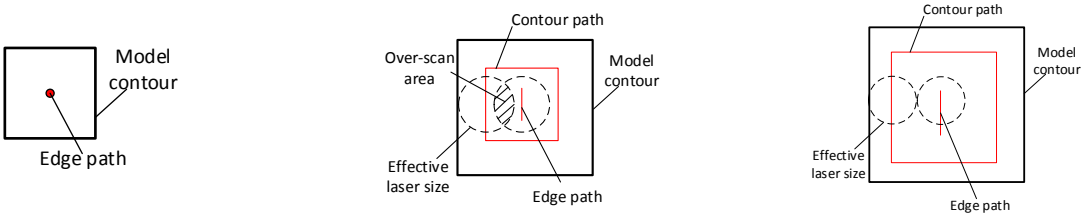

(a) 0.1mm (b) 0.2mm (c) 0.3mm

Fig.13 Scanning path overlap for different features by the contour+edge scanning method

Careful dimensional measurements were performed, and the results were compared with the designed dimensions for accuracy analysis. Fig.14 shows the dimensional accuracy of 2D thin features fabricated with higher energy density (0.195J/mm^2) by both contour+hatch and contour+edge scanning methods, and Fig.15 shows the dimensional accuracy of 2D thin features fabricated with lower energy density (0.13J/mm^2) by both contour+hatch and contour+edge scanning methods. The lower energy density group appears to result in more accurate feature dimensions, although this difference is not as significant for very small features. On the other hand, laser energy appears to have significant effect on the feature size accuracy, with 60W resulting in the best accuracy at all sizes. It is also worth noting that at relatively large sizes (0.3mm-0.5mm), the dimensional accuracy does not appear to have a single trend as a function of laser power. This might be due to the more complex melting pool dynamics at these process energy levels, which exceeded the scope of this study and will need to be investigated systematically in future studies. The results clearly suggested that the parameter combination of 60W + 385mm/s would be most suitable for 2D thin feature generation.

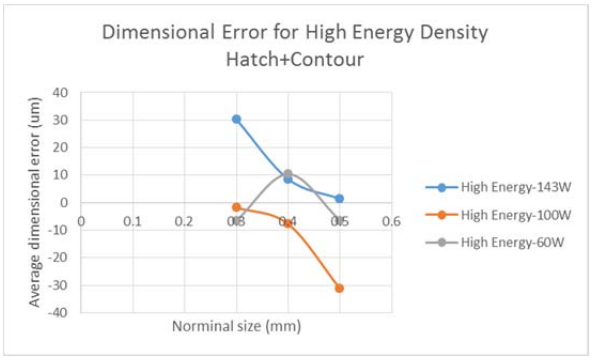

(a) Contour+hatch

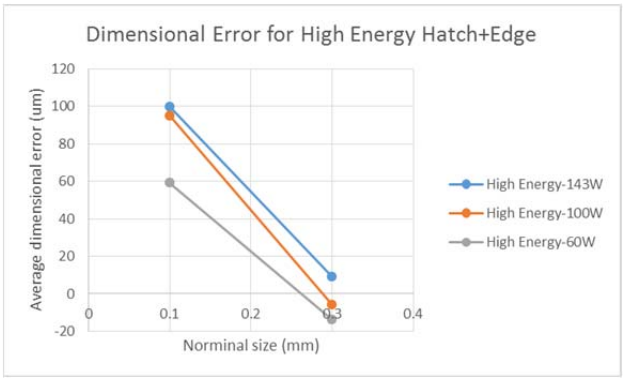

(b) Contour+edge

Fig.14 2D thin feature dimensional error with high energy density fabrication

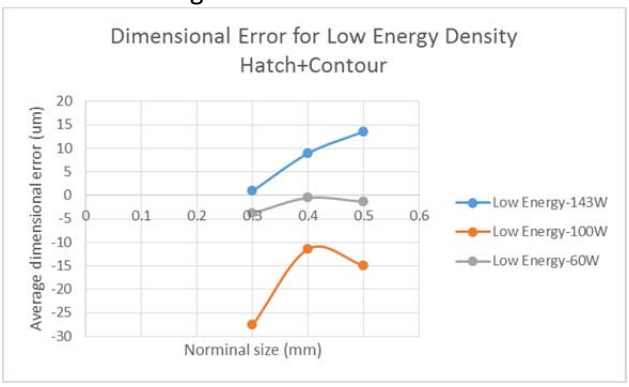

(a) Contour+hatch

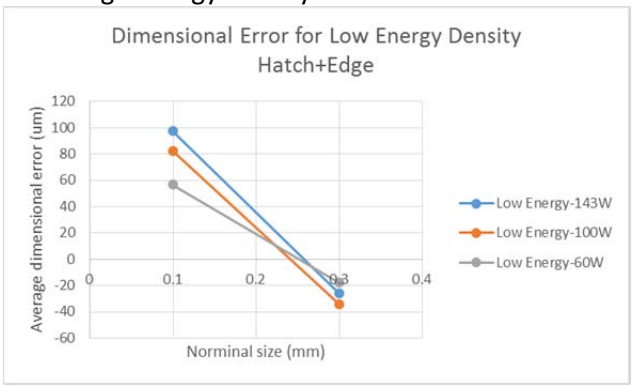

(b) Contour+edge

Fig.15 2D thin feature dimensional error with low energy density fabrication

Further inspections with the microstructure of the samples supported the suggestions that 60W+385mm/s is the optimum parameter for 2D thin feature generation. As shown in Fig.16 for 0.1mm features, with larger laser energy, the samples exhibit significant void defects located near the center of the cross section. This was likely a result of the excessive overheating at the center of the cross section and the subsequent difference of solidification time between the center region and the peripheral regions, which could potentially cause capillary force driven defects at the center. The same defects were also observed for 0.3mm features processed by the contour+edge method at higher beam energy levels, which is shown in Fig.17. This type of defect was completely absent for the same feature generated by the contour+hatch method. From a total energy input perspective the two methods were expected to yield similar results, therefore it was speculated that the sequence of scanning might be responsible for the difference. With the contour+hatch method, the hatch paths were scanned first, followed by a post-contour, whereas for the contour+edge, it could not be determined whether the contour path was scanned first. The difference in scanning sequence could lead to the change of thermal history and melting pool evolution in the scanned area, and potentially cause the observed defects.

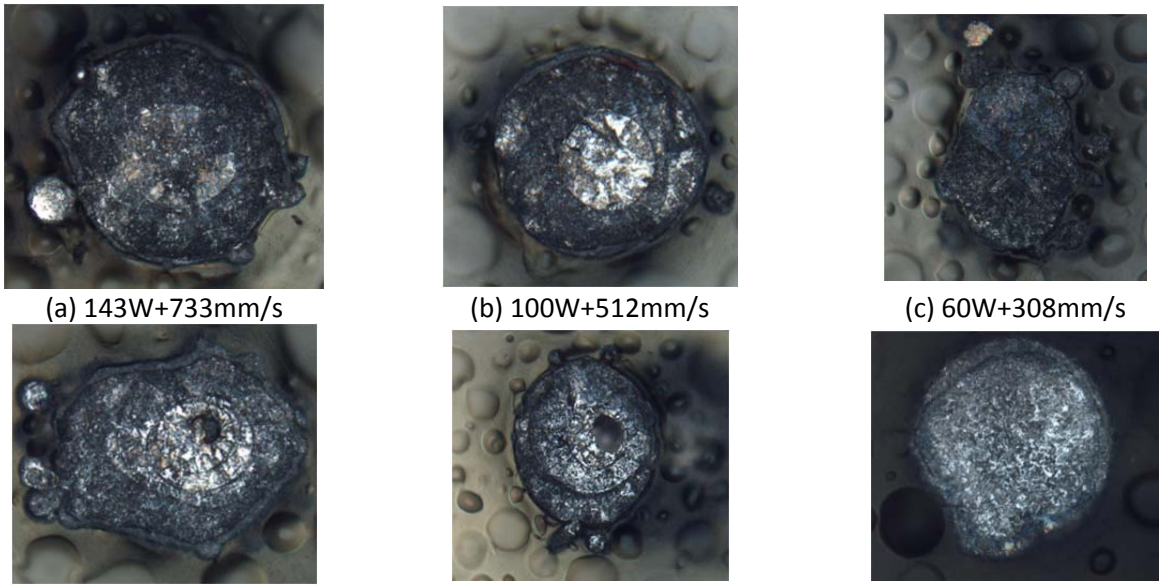

(a) 143W+733mm/s (b) 100W+512mm/s (c) 60W+308mm/s

(d) 143W+1100mm/s (e) 100W+770mm/s (f) 60W+385mm/s

Fig.16 Cross sectional microscopy of 0.1mm 2D thin features

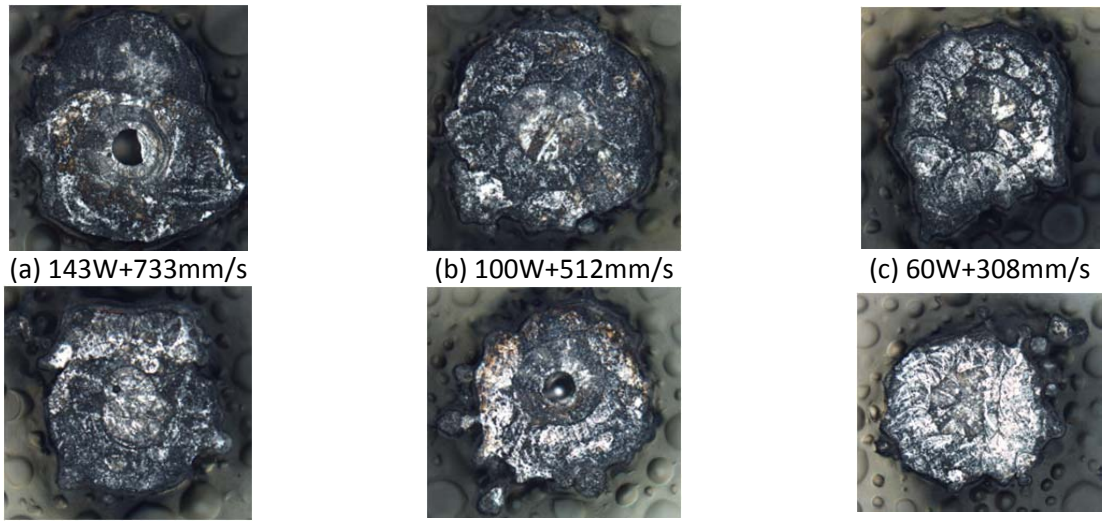

(a) 143W+733mm/s (b) 100W+512mm/s (c) 60W+308mm/s

(d) 143W+1100mm/s (e) 100W+770mm/s (f) 60W+385mm/s

Fig.17 Cross sectional microscopy of 0.3mm 2D features by contour+edge method

For the 1D thin features, the features generated by 60W laser power also exhibited the highest accuracy as shown in Fig.18. Also, for these features, the contour+edge method appeared to yield better accuracy compared to the contour+hatch method. Upon inspection of microstructure, it was found that lower energy density at 60W would result in internal voids and slight track instability, as shown in Fig.19. Therefore, slightly higher energy density is required for the generation of 1D thin features compared to 2D thin features, which is reasonable considering that the heat dissipation is two dimensional in thin wall features and only one dimensional in thin strut features. A thin wall feature of 80μm was obtained

with the 60W+308mm/s process parameter, which was significantly smaller compared to the support structures generated by the default EOS parameter.

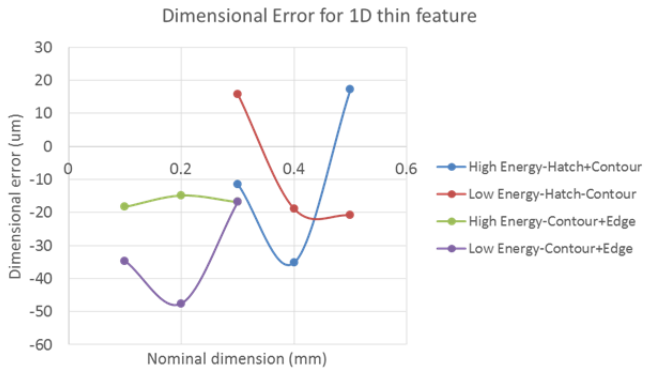

Fig.18 1D thin feature dimensional error with different process setting

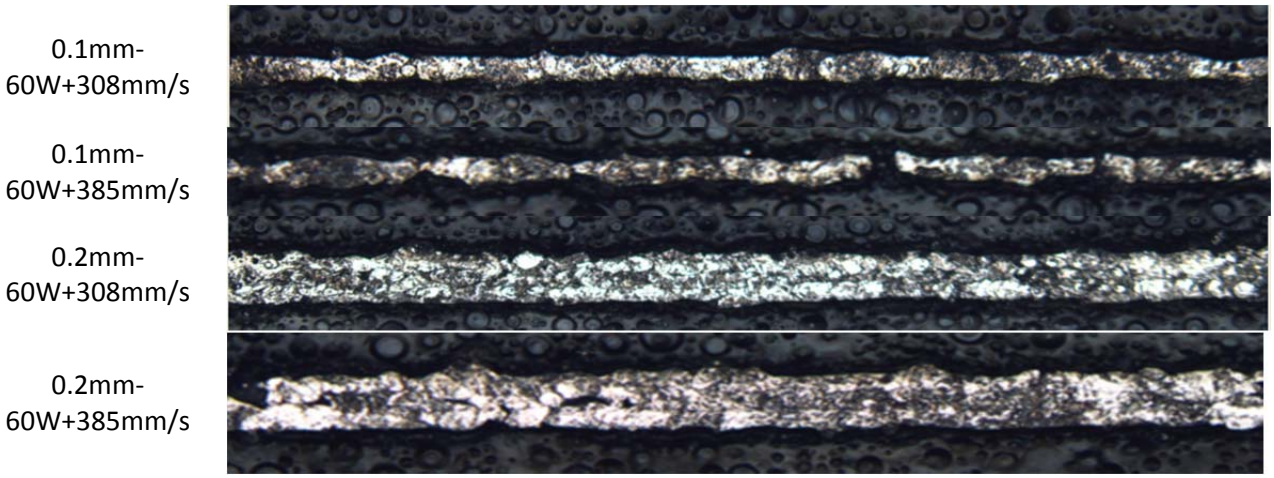

Fig.19 Cross sectional microscopy of 1D thin features with different process setting

Conclusions

Through this study it was revealed that there exist significant difference between the ways the DMLS process should be controlled for thin feature structures and regular bulky structures. A comprehensive study is likely needed to adequately address this new area of process development for powder bed fusion AM systems. Due to significant change in thermal history with altered heat dissipation conditions, the stability of the melt pool and the quality of the thin feature also requires extensive analysis by experimentation and simulation, which will need to be carried out in future studies. It was found that the current default support parameter used by EOS could potentially be further optimized to generate thinner wall structures, however, further experiments are needed to identify mechanical properties of these structures and establish their relationship with the process parameters.

Reference

[1] Case study from the Additive Manufacturing Products Division H-5800-0954-02-D: First metal 3D printed bicycle frame manufactured by Renishaw for Empire Cycles. Renishaw, 2014.

[2] Li Yang, Ola Harrysson, Harvey West, Denis Cormier. A comparison of bending properties for cellular core sandwich panels. Materials Sciences and Applications. 4(2013), 8: 471-477.

[3] Arcam Orthopedic Implants Solution. http://www.arcam.com/solutions/orthopedic-implants/.

[4] Denis Cormier, Harvey West, Ola Harrysson, Kyle Knowlson. Characterization of thin walled Ti-6Al-4V components produced via electron beam melting. Proceedings of the Solid Freeform Fabrication Symposium, Austin, TX, USA. 2004.

[5] L. E. Murr, S. M. Gaytan, F. Medina, E. Martinez, J. L. Martinez, D. H. Hernandez, B. I. Machado, D. A. Ramirez, R. B. Wicker. Characterization of Ti-6Al-4V open cellular foams fabricated by additive manufacturing using electron beam melting. Materials Science and Engineering A. 527(2010): 1861-1868.

[6] Li Yang. Structural design, optimization and application of 3D re-entrant auxetic structures. PhD Dissertation. North Carolina State University. Raleigh, NC, USA. 2011.

[7] S. J. Li, L. E. Murr, X. Y. Cheng, Z. B. Zhang, Y. L. Hao, R. Yang, F. Medina, R. B. Wicker. Compression fatigue behavior of Ti-6Al-4V mesh arrays fabricated by electron beam melting. Acta Materialia. 6092012): 793-802.

[8] R. Gumruk, R. A. W. Mines. Compressive behaviour of stainless steel micro-lattice structures. International Journal of Mechanical Sciences. 68(2013): 125-39.

[9] Chunze Yan, Liang Hao, Ahmed Hussein, David Raymont. Evaluations of cellular lattice structures manufactured using selective laser melting. International Journal of Machine Tools & Manufacture. 62(2012): 32-38.

[10] Li Yang, Ola Harrysson, Denis Cormier, Harvey West. Compressive properties of Ti6Al4V auxetic mesh structures made by electron beam melting. Acta Materialia. 60(2012): 3370-3379.

[11] Li Yang, Denis Cormier, Harvey West, Kyle Knowlson. Non-stochastic Ti6Al4V foam structure that shows negative Poisson's Ratios. Materials Science and Engineering A. 558(2012): 579-585.

[12] Li Yang, Ola Harrysson, Denis Cormier, Harvey West. Modeling of the uniaxial compression of a 3D periodic re-entrant honeycomb structure. Journal of Materials Science. 48(2013): 1413-1422.

[13] J. Schwerdtfeger, P. Heinl, R. F. Singer, C. Korner. Auxetic cellular structures through selective electron-beam melting. Physics Status Solidi B. 247(2010), 2: 269-272.

[14] Y. Shen. S. McKown, S. Tsopanos, C. J. Sutcliffe, R. A. W. Mines, W. J. Cantwell. The mechanical properties of sandwich structures based on metal lattice architectures. Journal of Sandwich Structures and Materials. 12(2010), 2: 159-180.

[15] Peter Heinl, Carolin Korner, Robert F. Singer. Selective electron beam melting of cellular titanium: mechanical properties. Advanced Engineering Materials. 10(2008), 9: 882-888.

[16] Peter Heinl, Andreas Rottmair, Carolin Korner, Robert F. Singer. Cellular titanium by selective electron beam melting. Advanced Engineering Materials. 9(2007), 5: 360-364.

[17] D. A. Ramirez, L. E. Murr, S. J. Li, Y. X. Tian, E. Martinez, J. L. Martinez, B. I. Machado, S. M. Gaytan, F. Medina, R. B. Wicker. Open-cellular copper structures fabricated by additive manufacturing using electron beam melting. Materials Science and Engineering A. 528(2011): 5379-5386.

[18] Dirk A. Hollander, Matthias von Walter, Tobias Wirtz, Richard Sellei, Bernhard Scvhmidt-Rohlfing, Othmar Paar, Hans-Josef Erli. Structural, mechanical and in vitro characterization of individually structured Ti-6Al-4V produced by direct laser forming. Biomaterials. 27(2006): 955-963.

[19] R. Stamp, P. Fox, W. O'Neill, E. Jones, C. Sutcliffe. The development of a scanning strategy for the manufacture of porous biomaterials by selective laser melting. Journal of Materials Science: Materials in Medicine. 20(2009): 1839-1848.

[20] S. Tsopanos, R. A. W. Mines, S. McKown, Y. Shen, W. J. Cantwell, W. Brooks, C. J. Sutcliffe. The influence of processing parameters on the mechanical properties of selectively laser melted stainless steel microlattice structures. Journal of Manufacturing Science and Engineering. 132(2010): 041011.

[21] I. Yadroitsev, Ph. Bertrand, I. Smurov. Parametric analysis of the selective laser melting process. Applied Surface Science. 253(2007): 8064-8069.

[22] Ola L. A. Harrysson, Omer Cansizoglu, Denis J. Marcellin-Little, Denis R. Cormier, Harvery A. West II. Direct metal fabrication of titanium implants with tailored materials and mechanical properties using electron beam melting technology.